J. Fluid Mech. (1981), *vol.* 110, *pp.* 97–113
Printed in Great Britain

Laminar gravitational convection of heat in dead-end channels

By TERRY W. STURM

School of Civil Engineering,
Georgia Institute of Technology,
Atlanta, Georgia

(Received 7 January 1980 and in revised form 1 December 1980)

A closed-form solution of the coupled momentum and thermal energy equations is obtained for laminar gravitational circulation of water resulting from a longitudinal temperature gradient in a dead-end channel. The temperature gradient is determined by the rate of heat loss from the water surface. The solution is shown to be dependent on a modified Rayleigh number which involves the local surface heat-transfer coefficient. An experimental study was conducted, and the results are compared with the closed-form solution.

1. Introduction

Gravity currents are an important phenomenon in environmental fluid mechanics. The distinguishing characteristic of gravity currents is that they are driven by a buoyancy which is the result of a density gradient in a gravitational field. This paper deals with thermally induced density gradients that occur in cooling lakes, which are large, confined bodies of water that receive waste-heat discharges. The resulting gravity currents are of particular interest in dead-end channels that form a portion of a natural lake. The gravitational circulation tends to draw heated water into 'stagnant' areas of the lake where it undergoes surface cooling that sustains the circulation.

Benjamin (1968) has clearly demonstrated the role of gravity in generating a streamwise pressure gradient where there exists a difference in fluid density in the direction of flow. This manifestation of the gravity force is distinct from its role as a body force. Even though the channel slope is zero with a resulting zero component of the body force in the direction of flow, buoyancy can drive a circulation as in the familiar example of lock-exchange flow between fresh-water and saline-water canals (Keulegan 1957).

The work by Phillips (1966) on the gravitational circulation of the Red Sea showed that a similarity solution of the turbulent equations of motion is possible when the surface buoyancy flux due to salt and heat flux is considered to be independent of the streamwise co-ordinate. Imberger (1974) studied laminar gravitational circulation experimentally, but in his case the end walls of the channel were differentially heated and the flow was confined at the top by an insulated lid. In a companion theoretical investigation of this problem, Cormack, Leal & Imberger (1974) applied an asymptotic analysis to the case of fixed Rayleigh number with the aspect ratio of the enclosed cavity approaching zero. Their analysis indicated the existence of a parallel flow structure in the core of the cavity.

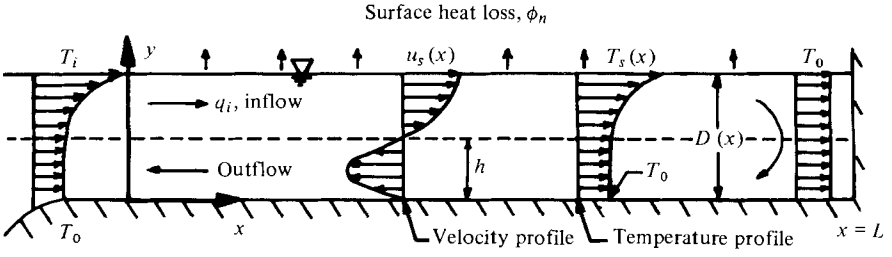

FIGURE 1. Vertical section of gravitational circulation in dead-end channel.

The essential aspect of the gravity currents considered herein is the continuous change in the thermally induced density gradient in the direction of flow as controlled by the heat-transfer process at the free surface. This type of gravitational circulation depends upon the coupling between the equations of motion and the equation of thermal energy conservation. The surface heat flux is not only a component in the thermal energy balance but determines the horizontal pressure gradient in the equations of motion as well.

Gravity currents which are the result of thermally induced density gradients that are diminished by surface heat flux have been studied experimentally by Brocard, Jirka & Harleman (1977) and by the author (Sturm 1976). The analytical work by the author (Sturm 1976) led to a numerical solution of the governing equations of motion and thermal energy for both laminar and turbulent circulations. A study of the reasonableness of the numerical solutions and the occurrence of the laminar regime in the laboratory provided the impetus to seek a closed-form solution for the laminar case.

2. Formulation

The problem is formulated with reference to the dead-end channel sketched in figure 1. The channel is assumed to have a horizontal bottom, a uniform width b, length L, and depth $D(x)$, where the co-ordinate system is defined in the figure. At the entrance to the channel ($x = 0$), there is a vertically non-uniform temperature profile with a surface temperature $T_s = T_i$ and a bottom temperature $= T_0$. Based on the experiments of the author (Sturm 1976), which will be discussed subsequently, it can be assumed that the temperature reached by the surface inflow current at the dead end of the channel becomes equal to the constant temperature T_0 of the bottom outflow current.

The surface heat-loss rate, ϕ_n, depends on the water surface temperature, T_s, and decreases with x as surface cooling occurs in the inflow current shown in figure 1. If essentially parallel flow is considered to exist in a central region of the channel, then a comparison of the hydrostatic pressure distributions at each end of this central region reveals a net force directed toward the open end of the channel. This force propels the bottom outflow current in figure 1. Continuity requires an equal but opposite inflow current which rides over the top of the outflow current. The inflow current must be driven by a drop in the free surface toward the dead end of the channel. The central region of the channel is bounded by a flow-establishment region near the

channel entrance in which inertia and buoyancy forces are dominant, and a dead-end region which is characterized by a large vertical downflow as the inflow current is turned. The analysis herein is concerned primarily with the central region of a dead-end channel with large length-to-depth ratio in which the flow is nearly parallel and governed by buoyancy and viscous forces.

The equations of motion and thermal energy conservation are simplified by making the following assumptions: (1) the flow is laminar; (2) the dead-end channel has a large length-to-depth ratio (small aspect ratio); (3) the rate of surface heat loss, ϕ_n, can be related linearly to the excess surface temperature relative to an equilibrium temperature, T_e, e.g. $\phi_n = -K(T_s - T_e)$; (4) the vertical temperature profile shape is known and can be expressed by $\theta = (T - T_0)/(T_s - T_0) = f_T(\eta)$, where $\eta = y/D$; (5) the temperature *vs.* density relation is approximately linear over the surface temperature range, $(T_i - T_0)$; and (6) the Boussinesq assumption applies.

Although the assumption of laminar flow may be unrealistic except in laboratory situations, it is made in order to gain some insight into the more complex dynamics of turbulent gravity currents, which occur in cooling lakes. In the central region of the flow, which is relatively very long in comparison to the depth as supposed by assumption (2), boundary-layer-type simplifications become possible in the equations of motion and thermal energy. The linear relation for ϕ_n in assumption (3) is based on an equilibrium temperature, T_e, such that when $T_s = T_e$, there is no net surface heat flux. The coefficient, K, and T_e are functions of meteorological conditions and the surface temperature at $x = 0, T_i$. They can be determined by the empirical relations summarized by Ryan, Harleman & Stolzenbach (1977) for the relevant processes of heat transfer at the air–water interface. Assumption (4) concerning the temperature profile shape is similar to that employed in the Kármán–Pohlhausen type of boundary-layer analysis in which the integral properties of the flow in the vertical direction are retained to effect a solution with respect to the horizontal, streamwise co-ordinate.

With the above assumptions, the coupled equations of motion and thermal energy become:

$$\rho_0 \left(u \frac{\partial u}{\partial x} + v \frac{\partial u}{\partial y} \right) = -\frac{\partial p}{\partial x} + \mu \frac{\partial^2 u}{\partial y^2}, \tag{1}$$

$$\frac{\partial p}{\partial y} = -\rho g = -g(\alpha T + \beta), \tag{2}$$

$$\frac{d}{dx} \int_0^D uT \, dy = \frac{-K}{\rho_0 c_p} (T_s - T_e), \tag{3}$$

in which ρ_0 is a reference density corresponding to the temperature, T_0, and α is the slope of the density *vs.* temperature relation. The thermal energy equation, (3), has been written in integral form by applying the continuity equation and integrating over the depth with a boundary condition of zero heat flux at $y = 0$, and with the heat flux being given by the assumed linear relation at the air–water interface ($y = D$).

The inertia terms have been retained in (1) based on a preliminary order-of-magnitude analysis, while the horizontal diffusive terms have been neglected in (1) and (3) in comparison with the corresponding vertical contributions because $L/D \gg 1$. A closer examination of the horizontally elongated central region of the dead-end channel, however, reveals that the inertia terms may make a sufficiently small

contribution to equation (1) to be neglected as a first approximation. If the channel is very long (i.e. sufficiently long that all excess heat is lost to the atmosphere), the longitudinal gradient of horizontal velocity is quite small as is the magnitude of the velocity itself. For a shorter channel which still has a large length-to-depth ratio, much of the inertia of the inflow current might be expected to be lost within a horizontal distance of a few depths from the dead end of the channel. In this end region, which is very short, the inertia of the inflow current is lost rapidly as the dead end is approached and the free surface rises. The inertia is regained as the outflow current accelerates from the dead end and flows in a direction opposite to that of the inflow current. Thus, in the central region of essentially parallel flow, the inertia terms may be sufficiently small, when compared with the buoyancy and viscous forces, to be neglected. This assumption cannot be verified *a priori* because a careful estimate of the velocity scale can only be made after a solution of this free-convection problem has been obtained.

Buoyant flows for which the formulation is given by (1)–(3), excluding the inertia terms in (1), have been classified by Turner (1973) as viscous diffusive flows. Turner points out that this type of flow can be characterized by a single dimensionless parameter, the Rayleigh number, which reflects the importance of diffusion as well as viscous and buoyancy forces. Such a formulation corresponds to Koh's (1966) zeroth-order approximation for the problem of viscous stratified flow towards a sink. As another example of this type of flow, data for free-convection heat transfer from horizontal cylinders in several different fluids are well correlated with the Rayleigh number as the only independent parameter (Kreith 1973).

As a first approximation, then, it is not without precedent nor lacking in at least some intuitive justification to neglect the inertia terms in (1) for the problem under consideration. This is done in the following section of this paper in which a closed-form solution of (1)–(3) is presented. The limitations of this assumption will be analysed in more detail in § 4.

3. Solution

The solution of (1), (2) and (3), with the inertia terms neglected in (1), proceeds by substituting the temperature profile function $f_T(\eta)$ into (2) and eliminating the pressure p from (1) and (2) to obtain:

$$\frac{\partial^2 u}{\partial y^2} = -\frac{\alpha g D}{\mu}\frac{d(T_s - T_0)}{dx}\int_1^\eta f_T(\eta)\,d\eta + \frac{g(\alpha T_0 + \beta)}{\mu}\frac{dD}{dx}. \tag{4}$$

Equation 4 is integrated with the boundary conditions $u = 0$ at $y = 0$ and $\partial u/\partial y = 0$ at $y = D$ to produce the velocity distribution:

$$u = \frac{\alpha g D^3}{\mu}\frac{d(T_s - T_0)}{dx} f_u(\eta), \tag{5}$$

where dD/dx has been expressed in terms of the temperature gradient, $d(T_s - T_0)/dx$, by applying the continuity condition,

$$\int_0^1 u\,d\eta = 0.$$

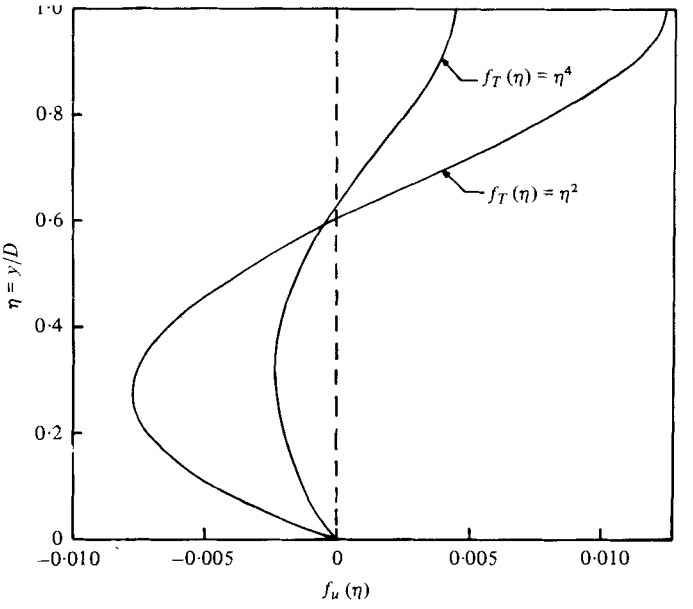

FIGURE 2. Velocity profile polynomials $f_u(\eta)$ for selected temperature profile polynomials $f_T(\eta)$.

The function $f_u(\eta)$ in (5) is a velocity profile function determined solely by the choice of the temperature profile shape, $f_T(\eta)$. In figure 2, $f_u(\eta)$ is shown for $f_T(\eta) = \eta^2$ and $f_T(\eta) = \eta^4$. The postulated counter-flow is readily evident from the shape of $f_u(\eta)$. The elevation of zero velocity between the inflow and outflow currents is relatively insensitive to the choice of $f_T(\eta)$, but the magnitude of $f_u(\eta)$ decreases at all elevations with an increase in the degree of the temperature profile polynomial, $f_T(\eta)$.

The solution given by (5) for the velocity u was obtained solely from momentum and continuity considerations, and it involves the surface temperature gradient, $d(T_s - T_0)/dx$, as an unknown parameter. This parameter couples the momentum equation to the thermal energy equation. If (5) is substituted into (3), which is the thermal energy equation, along with the assumed temperature profile $f_T(\eta)$, then there results an ordinary differential equation in the unknown $(T_s - T_0)$. In dimensionless form, the equation to be solved is:

$$\theta_s \frac{d^2\theta_s}{dx^{02}} + \left(\frac{d\theta_s}{dx^0}\right)^2 - B_1\theta_s - \frac{B_1\theta_0}{(1-\theta_0)} = 0, \tag{6}$$

where

$$x^0 = \frac{x}{D}, \quad \theta_s = \frac{(T_s - T_0)}{(T_i - T_0)}, \quad \theta_0 = \frac{(T_0 - T_e)}{(T_i - T_e)},$$

$$B_1 = \frac{C_1}{Ra_m(1-\theta_0)}, \quad Ra_m = \frac{(\Delta\rho_e/\rho_e)gD_i^2}{\nu K/\rho_e c_p},$$

and where an i subscript refers to values at $x = 0$, ν is kinematic viscosity, K is the local surface heat transfer coefficient, c_p is specific heat, g is gravitational acceleration,

C_1 is a temperature profile constant defined in the appendix, $\Delta\rho_e = \rho(T_e) - \rho(T_i)$, $\rho_e = \rho(T_e)$, and the various temperatures are defined in figure 1.

The governing dimensionless parameter in (6) is a modified form of the Rayleigh number, Ra_m, in which the thermal conductivity has been replaced by KD_i. The local coefficient of heat transfer $K[= -\phi_n/(T_s - T_e)]$ characterizes all the heat-transfer processes at the air–water interface including evaporation, conduction and radiation. The modified Rayleigh number can be considered to be a product of the Grashof number and a modified Prandtl number given by $\mu c_p/KD_i$. The additional parameter appearing in (6) is θ_0, which is the unknown temperature boundary condition at $x = L$, where L is the channel length. It will be shown below that θ_0 can be determined as a function of L, D_i and Ra_m.

An exact solution can be obtained for (6) by making the substitution of variables $\chi = d\theta_s/dx^0$ with θ_s becoming the independent variable and χ the dependent variable. Exact integration of (6) with the boundary conditions $\theta_s = 1$ at $x^0 = 0$ and $d\theta_s/dx^0$ finite as θ_s approaches zero provides the solution for the dimensionless temperature, velocity and depth:

$$\theta_s = \frac{T_s - T_0}{T_i - T_0} = \frac{B_1}{6} x^{02} - B_2 x^0 + 1, \tag{7}$$

$$U_{si} = \frac{u_s}{u_{si}} = 1 - \frac{B_1}{3B_2} x^0, \tag{8}$$

$$\delta = \frac{D(x)}{D_i} = 1 - C_2 \frac{\Delta\rho_0}{\rho_0} x^0 \left[B_2 - \frac{B_1}{6} x^0 \right], \tag{9}$$

where

$$B_2 = \left(\frac{B_1^2 L^{02}}{36} + \frac{B_1}{3} + \frac{1}{L^{02}} \right)^{\frac{1}{2}},$$

and where $L^0 = L/D_i$, C_2 is a temperature profile constant defined in the appendix, $\Delta\rho_0 = \rho(T_0) - \rho(T_i)$; the other variables have been defined previously. The solution given by (8) for U_s is determined by differentiating (7) with respect to x^0 and substituting the result into (5). The continuity condition and the integrated form of (4) provide the necessary relation between $d\theta_s/dx^0$ and $d\delta/dx^0$ from which (9) is obtained.

The solutions given by (7), (8) and (9) are not complete without the boundary values of the surface velocity at $x = 0$, u_{si}, and the surface temperature at $x = L$, T_0. These must be determined from the imposed physical conditions of channel length, depth, surface temperature at the channel entrance, and meteorology.

The unknown boundary condition θ_0 for a channel of given length L is determined by setting $T_s = T_0$ at $x = L$ in (7) and expressing the result in terms of the ratio $\gamma = L/L_e$, where L_e is an equilibrium length:

$$\theta_0 = 1 + 2\gamma^2 - \gamma(6 + 3\gamma^2)^{\frac{1}{2}}. \tag{10}$$

The equilibrium length is defined to be the length of channel required for the surface temperature T_s to become equal to T_e, the equilibrium temperature, at which the net surface heat exchange is zero. The equilibrium length is determined from (7) as the value of x for which $T_s = T_0 = T_e$:

$$\frac{L_e}{D_i} = \left(\frac{6Ra_m}{C_1} \right)^{\frac{1}{2}}. \tag{11}$$

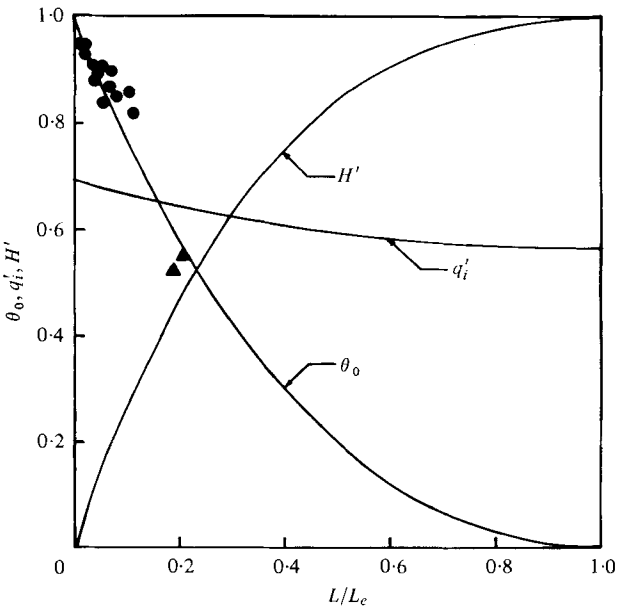

FIGURE 3. Solutions for dimensionless bottom temperature, entrance flow rate and surface heat-loss rate for channel of length L. Equilibrium length L_e is given by (11). ▲, experimental values for θ_0 by the author [$f_T(\eta) = \eta^5$]; ●, experimental values for θ_0 by Brocard *et al.* (1977) [$f_T(\eta) = \eta^4$].

It is now apparent from (10) and (11) that the dimensionless boundary value given by θ_0 is a function only of L/D_i, the Rayleigh number, and the profile constant C_1.

The inlet surface velocity, u_{si}, is easily determined from (5) and (7):

$$\frac{u_{si}}{K/\rho_e c_p} = C_3 \frac{B_2}{B_1}, \tag{12}$$

where C_3 is another temperature profile constant defined in the appendix, and B_2 and B_1 are as defined before. For the purpose of later comparison with experimental data, it is more convenient to use an expression for the inflow per unit width into the channel, q_i:

$$q_i' = \frac{q_i}{(KL_e/\rho_e c_p)} = C_4 \frac{B_2}{B_1 L_e^0}, \tag{13}$$

where C_4 is defined in the appendix and $L_e^0 = L_e/D_i$. It can also be shown that $B_2/B_1 L_e^0$ and hence q_i' are functions only of $\gamma = L/L_e$ just as for θ_0.

Although the solution of (1), (2) and (3) is now complete, one of the quantities of interest may be the total rate of surface heat loss from the channel, which can be determined from the foregoing development. If the total rate of surface heat loss H_E from a channel of equilibrium length and width b is defined as

$$H_E = b \int_0^{L_e} \phi_n \, dx = \bar{h}_c b L_e (T_i - T_e), \tag{14}$$

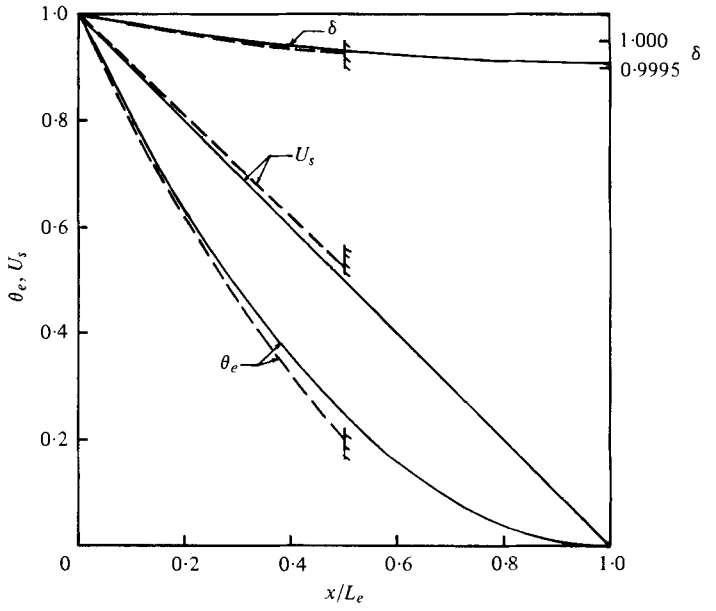

FIGURE 4. Solutions for surface velocity, temperature and depth variation with longitudinal distance along the channel for $L/L_e = 1{\cdot}0$ (——) and $L/L_e = 0{\cdot}5$ (– – –). $\theta_e = (T_s - T_i)/(T_i - T_e) = \theta_s(1-\theta_0)+\theta_0$; $U_s = u_s/u_{si}$; $\delta = D(x)/D_i$.

it is readily shown that $\bar{h}_c = \frac{1}{3}K$ from a substitution of (7) into (14). For a channel of specified length L, the ratio of surface heat-loss rate H_L to that from the equilibrium channel of length L_e is formed and found to be a function of $\gamma = L/L_e$:

$$H' = \frac{H_L}{H_E} = 3\gamma\left[1+\frac{\gamma^2}{3}-\left(\gamma^4+\frac{3\gamma^2}{2}-\frac{\gamma^3}{2}(6+3\gamma^2)^{\frac{1}{2}}\right)^{\frac{1}{2}}\right]. \tag{15}$$

The solutions for θ_0, q_i' and H' are shown in figure 3 as a function of γ.

The profile constants that appear in the solution are given in table 1 for several polynomial temperature profile shapes. The shapes chosen are $f_T(\eta) = \eta^m$, where m varies from 1 to 5. These functions were selected for ease of integration. Other functions are possible, and the resulting constants can be evaluated from the expressions given in the appendix. Because of the way in which the surface heat-transfer boundary condition is specified in the integral solution approach, it is unnecessary for the assumed temperature profile shape to have the correct slope at the free surface.

4. Discussion of solution

Introduction of the equilibrium length L_e provides a useful generalization of the dimensionless solutions for surface temperature, velocity, and depth in (7), (8) and (9), in which the independent variable is x/D_i. If the solutions are plotted *vs.* x/L_e instead of x/D_i, they become universal in form as shown in figure 4. The terms involving only B_1, B_2 and x^0 in (7), (8) and (9) can be shown to reduce to functions of x/L_e and L/L_e. The dependence on Ra_m and the temperature profile shape is embedded in L_e such that specifying L/L_e establishes the complete solution for dimen-

sionless temperature and velocity in figure 4. The solution for the dimensionless depth in figure 4 further requires the value of $\Delta\rho_0/\rho_0$ as can be observed from (9). Although $\Delta\rho/\rho_0$ can be determined from $(T_i - T_0)$, the relation between θ_0 and L/L_e is insufficient to obtain $(T_i - T_0)$. The value of $(T_i - T_e)$ is also needed because of the non-dimensionalization inherent in the definition of θ_0. For the non-dimensional depth solution, then, $(T_i - T_e)$ must be specified in addition to L/L_e. This does not decrease the generality of the solution because $(T_i - T_e)$ must also be known to calculate Ra_m and hence L/L_e. The equilibrium temperature, T_e, depends only on meteorological conditions, while T_i is the surface temperature at the entrance of the channel and must be specified.

The solutions for $L/L_e = 1{\cdot}0$ and $0{\cdot}5$ are compared in figure 4. As the channel length is decreased while holding constant all other variables, the velocity at $x = 0$ increases owing to reduced overall friction in spite of the decrease in the hydrostatic force as T_0 increases. Simultaneously, the horizontal temperature gradient at $x = 0$ becomes larger negatively so that heat conservation is satisfied; the net heat flux into the channel must equal the total heat flux from the water surface at steady state. The boundary values T_0 and u_{si} adjust themselves as the channel length decreases such that both the thermal energy and momentum equations are satisfied.

The solutions shown in figure 4 are affected by the choice of temperature profile shape only through a change in equilibrium length L_e. It was shown in figure 2 that, as the degree n of the temperature profile polynomial increases, the resulting velocity polynomial, $f_u(\eta)$, decreases in magnitude over the full depth of flow. For a channel of given length and specified value of Ra_m, the surface velocity at $x = 0$, u_{si}, becomes smaller as n increases because of the decrease in the buoyant force arising from the hydrostatic pressure force difference between the entrance and the dead end of the channel. Consequently, there is a decrease in the net heat transported into the channel and a greater surface temperature drop, $(T_i - T_0)$, over the full length of the dead end channel. These effects are reflected in figure 4 by a decrease in the equilibrium length.

The depth decreases toward the dead end of the channel as shown in figure 4 in order to drive the inflow current as postulated in § 2. Although the depth change is very small, it makes a significant contribution to the horizontal pressure gradient and thus to the magnitude of the velocity at any x. As the contribution of the horizontal temperature gradient to the pressure gradient goes to zero for x/L_e approaching $1{\cdot}0$, so also does the contribution of the depth gradient. For a channel of given length $L < L_e$, the depth will increase with x as the surface temperature T_s approaches T_0 so that the velocity can be forced to zero as the dead end is reached. This depth increase will occur over a relatively short reach of the channel near the dead end. Over this short reach, the formulation and solutions presented herein are not applicable.

The solutions for θ_0, q_i' and H' in figure 3 indicate how the boundary conditions and heat loss vary with the ratio L/L_e. The solutions themselves are practically insensitive to the temperature profile shape (see table 1 for variation in C_4 which appears in (13)), but the value of L_e is quite dependent on $f_T(\eta)$. The heat-loss rate increases very rapidly with γ. Approximately 83 per cent of the maximum possible rate of heat loss and 80 per cent of the maximum surface temperature drop occur in a channel which has a length that is only 50 per cent of the equilibrium length. As a result, the value of q_i' changes very little for $L/L_e > 0{\cdot}5$. For $L/L_e < 0{\cdot}5$, q_i' increases gradually with a decrease in channel length as discussed previously. The curve for θ_0 in figure 3 should not be interpreted as the rate at which the surface temperature

m	C_1	C_2	C_3	C_4	$f_u(\eta)$
1	576	0·275	7·20	1·60	$-\frac{\eta^4}{24}+\frac{9\eta^2}{80}-\frac{7\eta}{120}$
2	800	0·217	6·67	1·50	$-\frac{\eta^5}{60}+\frac{7\eta^2}{120}-\frac{\eta}{30}$
3	1200	0·179	7·14	1·57	$-\frac{\eta^6}{120}+\frac{3\eta^2}{84}-\frac{3\eta}{140}$
4	1764	0·152	7·88	1·68	$-\frac{\eta^7}{210}+\frac{27\eta^2}{1120}-\frac{5\eta}{336}$
5	2509	0·132	8·71	1·82	$-\frac{\eta^8}{336}+\frac{35\eta^2}{2016}-\frac{11\eta}{1008}$

TABLE 1. Solution profile constants and velocity functions for $f_T(\eta) = \eta^m$.

decreases with x for a given channel length, but rather as the locus of boundary values, T_0, for channels of variable length.

The concept of an equilibrium length was developed because of the generality it provides in the presentation of the solutions in figures 3 and 4. It is not intended to obscure the controlling dimensionless parameter of the free convection in the dead-end channel. This parameter is the modified Rayleigh number, Ra_m, which emphasizes the dominance of the buoyancy and viscous forces and the importance of surface heat transfer in a central region of the dead-end channel for which $L/D \gg 1$. Decreasing the fluid viscosity in a channel of given length, for example, increases Ra_m and L_e/D and, as a result, the inflow velocity increases while the surface temperature drop, $(T_i - T_0)$, decreases. On the other hand, increasing the surface heat transfer coefficient K decreases Ra_m, and $(T_i - T_0)$ increases. Thus, the modified Rayleigh number measures not only the relative importance of buoyancy and viscous forces but also the rate at which the driving buoyancy force is being lost by surface heat transfer to the atmosphere.

The limitations of neglecting the inertia terms in (1) can be examined in light of the closed-form solution which has been obtained. If the closed-form solution is utilized to provide a first-order estimate of the magnitude of the inertia terms, their relative importance when compared with the buoyancy and viscous terms in (1) can be assessed. The ratio of inertia to buoyancy forces is given by the following definition of densimetric Froude number, F:

$$F^2 = \frac{u_{si}(\Delta u_s/L)}{g(dD/dx)_i}, \tag{16}$$

in which u_{si} is the surface velocity at $x = 0$; Δu_s is the decrease in surface velocity from $x = 0$ to the end region (assumed to be very short) where $x = L$; and $(dD/dx)_i$ is the slope of the free surface at $x = 0$. The evaluation of F^2 has been chosen at a point where the inertia forces can be expected to have their maximum value. The buoyancy force at the free surface, where the inertia terms are evaluated, is contributed solely by the slope of the free surface that is necessary to balance the effect of the horizontal density gradient integrated over the depth.

If u_{si}, Δu_s, and $(dD/dx)_i$ are evaluated by the closed-form solution, the following expression is obtained for F^2:

$$F^2 = \frac{1}{Pr_m}\left(\frac{C_3^2}{3C_1C_2}\right), \tag{17}$$

in which C_1, C_2 and C_3 are profile constants given in table 1, and Pr_m is a modified Prandtl number defined by $\mu c_p/KD$, where K is the local coefficient of surface heat transfer, D is the depth, c_p is specific heat, and μ is absolute viscosity. If the inertia terms are indeed small, then $F^2 \ll 1$, which requires that $Pr_m \gg 8 \times 10^{-2}$. The choice of $m = 3$, 4 or 5 in table 1 gives virtually the same limiting value of Pr_m. Using typical values of $K = 2 \times 10^{-3}$ W cm^{-2} K^{-1} and $D = 20$ cm for laboratory conditions with water as the fluid, Pr_m has a value of approximately 1·0, which is at least one order of magnitude larger than the limit at which the inertia terms must be considered. Thus, it seems that, for Pr_m sufficiently large, it is possible to neglect the inertia terms in (1), at least as a first approximation.

On the other hand, the convective terms in the thermal energy equation, (3), cannot be neglected. The heat that is lost through the free surface must be balanced by the net longitudinal convection of heat. The vertical heat diffusion terms, which supply the heat to the free surface, must be much larger than the horizontal diffusion terms if $L/D \gg 1$ and, as a result, must be of the same order as the longitudinal convection terms. Imberger (1974) reports that, in the reduction of his experimental results for an enclosed cavity of small aspect ratio, the convective heat transfer far exceeded the horizontal conduction of heat. This is also true in the present situation in which the heat lost at the free surface is supplied by horizontal convection.

5. Experiments

Laboratory experiments were conducted in a tilting flume at the Iowa Institute of Hydraulic Research. The flume is 26 m long, 0·75 m wide, and has glass side walls which are 25 cm high. The flume was set at zero slope, and water was ponded in a 20 m length of the flume by placing aluminium bulkheads in it as shown in figure 5. Electric, immersion heating rods were positioned in the ponded water to serve as an artificial heat source. Temperatures and velocities were measured after steady state had been reached, which was typically 24 hours after the immersion heaters were started.

The temperature field was measured by a movable rake of thermistors connected to an IBM 1800 data acquisition and control system. Bridge voltages from the thermistors were digitized and converted to temperatures by means of stored calibration curves. The temperatures at each vertical position of the thermistor rake were width averaged and displayed an uncertainty of no more than $\pm 0{\cdot}1$ °C, which confirms the existence of a two-dimensional temperature field.

Velocity profiles were measured by photographing a vertical time line at the beginning and end of a measured time interval. Continuity checks in the inflow and outflow currents indicated an uncertainty of 10–20 per cent in the flowrate computed from measured velocities. This was to be expected because of the small magnitude of the velocities and attendant measurement difficulty.

The isotherms and representative temperature profiles for experimental runs A and B are shown in figures 6 and 7, respectively. In the central region of the channel,

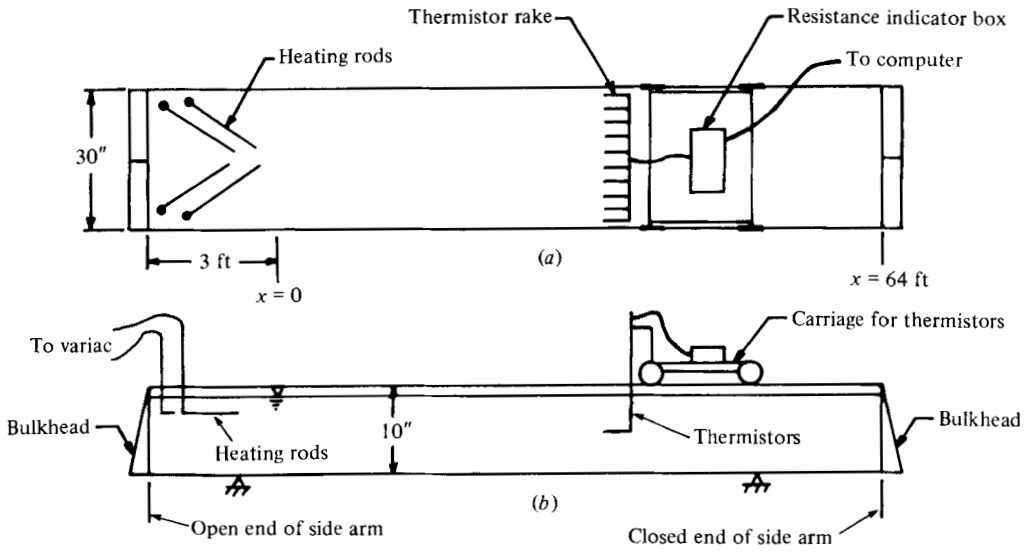

FIGURE 5. General layout of experimental dead-end channel. (*a*) Plan; (*b*) profile.

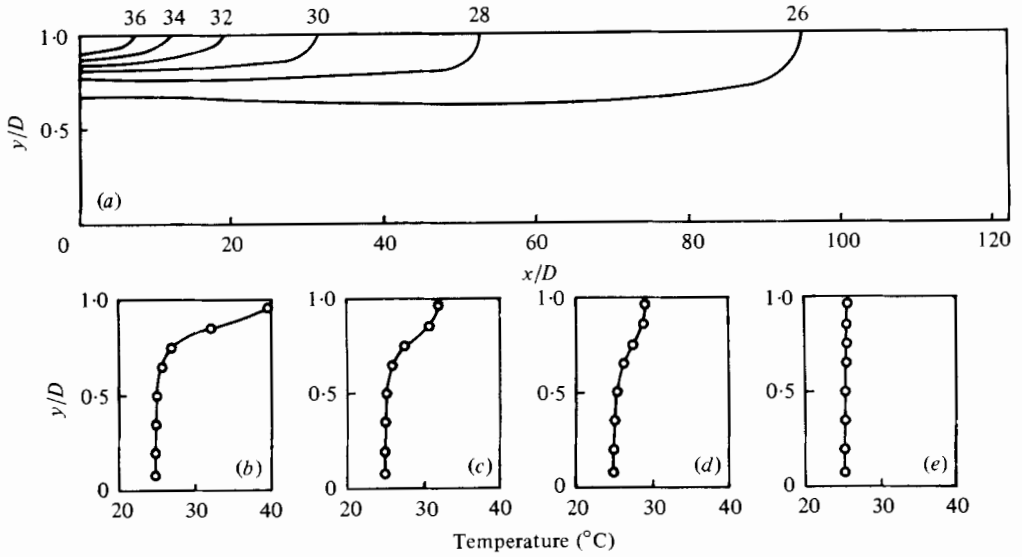

FIGURE 6. Isotherms and temperature profiles for experimental run *A*. (*a*) Isotherms (°C), (*b*) $x/D = 0$, (*c*) $x/D = 19$, (*d*) $x/D = 38$, (*e*) $x/D = 114$. $D = 16{\cdot}1$ cm, $T_e = 21{\cdot}1$ °C, $q_i = 1{\cdot}2$ cm^2 s^{-1}.

the isotherms are nearly horizontal and rise to the water surface as a result of surface cooling. Large vertical gradients of temperature in the upper half of the flow are apparent. The surface temperature decreases toward the dead end of the channel and reaches a value equal to the nearly constant bottom temperature.

A typical velocity profile is given in figure 8. There is a central region of the channel in which the point of zero velocity between inflow and outflow currents remains at a nearly constant elevation. Within this region the flow is practically parallel, and the

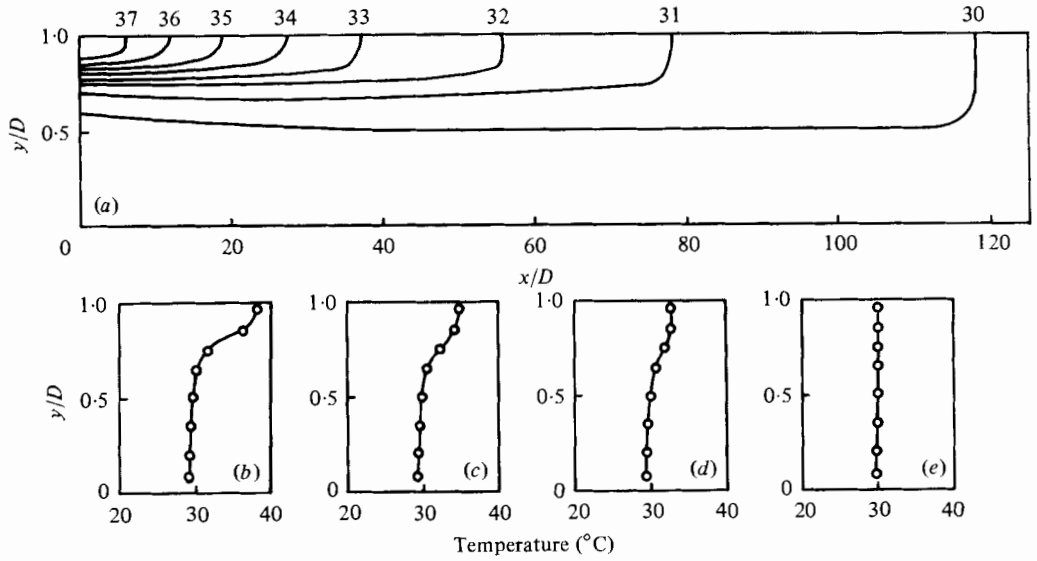

FIGURE 7. Isotherms and temperature profiles for experimental run *B*. (*a*) Isotherms (°C), (*b*) $x/D = 0$, (*c*) $x/D = 20$, (*d*) $x/D = 39$, (*e*) $x/D = 118$. $D = 15{\cdot}5$ cm, $T_e = 26{\cdot}4$ °C, $q_i = 1{\cdot}5$ cm^2 s^{-1}.

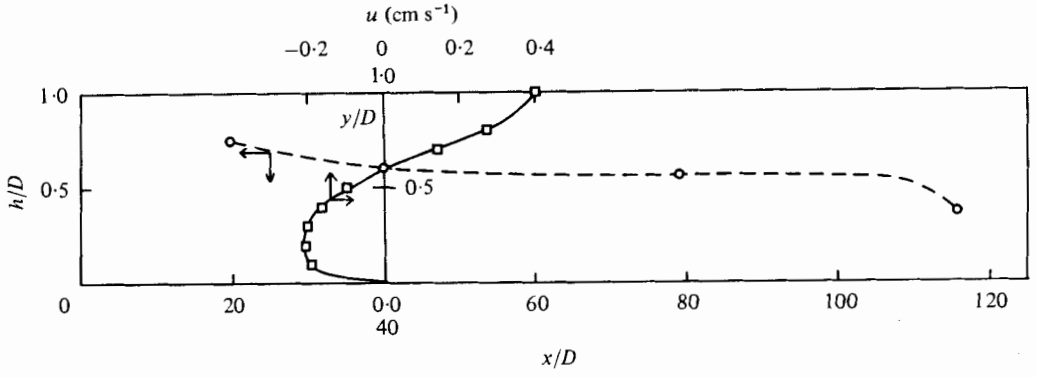

FIGURE 8. Measured velocity profile at $x/D = 40$ and measured height, h, of zero horizontal velocity along channel for experiment *B*. $D = 15{\cdot}5$ cm.

assumptions made to achieve a closed-form solution of the equations of motion and thermal energy are applicable. Upstream of this region is a region of flow establishment in which large vertical currents occurred as a result of the placement of the heating rods near the water surface.

6. Comparison of experimental results with solution

For the purpose of comparison with the closed-form solution, the experimental results of Brocard *et al.* (1977) as well as those of the present author are considered. The experiments by Brocard *et al.* (1977) were conducted in a 10·7 m long flume with

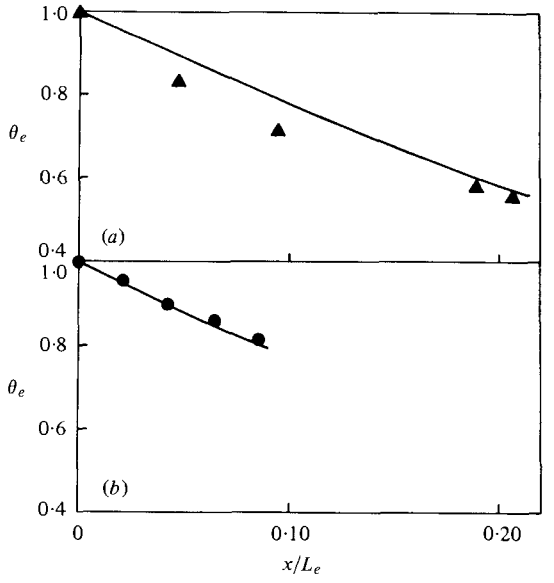

FIGURE 9. Comparison of closed-form solution (——) for longitudinal distribution of θ_e $[= (T_s - T_e)/(T_i - T_e)]$ with experimental values. (*a*) ▲, experiment *B*, $T_i = 32{\cdot}7$ °C, $T_e = 26{\cdot}4$ °C, $D = 15{\cdot}5$ cm, $L = 19{\cdot}5$ m, $Ra_m = 7{\cdot}2 \times 10^7$, $Pr_m = 0{\cdot}8$, $L_e/D = 415$ $[f_T(\eta) = \eta^5]$. (*b*) ●, experiment 14 (Brocard *et al.* 1975), $T_i = 42{\cdot}4$ °C, $T_e = 20{\cdot}8$ °C, $D = 16{\cdot}5$ cm, $L = 10{\cdot}6$ m, $Ra_m = 2{\cdot}3 \times 10^8$, $Pr_m = 0{\cdot}75$, $L_e/D = 742$ $[f_T(\eta) = \eta^5]$.

a head tank which was wider than the flume and into which heated water was introduced through a radial diffuser. An equal discharge of water was withdrawn through a multiport outlet device in the head tank. The resulting stratified temperature profile at the entrance to the channel produced a gravity circulation in the channel similar to that described herein for the author's experiments.

The distribution of surface temperature along the channel obtained from the closed-form solution is compared with the author's experimental run *B* and with experimental run 14 of Brocard, Jirka & Harleman (1975) in figure 9. For both runs, the temperature profile polynomial has been assumed to be $f_T(\eta) = \eta^5$ because the temperature profiles were similar in shape. The height of the inflection point in the temperature profile (measured above the channel bottom) was 0·75 times the depth for run *B* and 0·70 times the depth for run 14. Only the downstream 13 m of the channel in run *B* are included in the central region due to the vertical currents that occurred in the region of flow establishment. It can be seen in figure 9 that the agreement with the closed-form solution is much better for run 14 than for run *B*. A portion of the discrepancy in run *B* may be attributed to a surface heat-loss relationship which was highly nonlinear.

Much of the data presented by Brocard *et al.* (1977) is for the boundary values θ_0 and a dimensionless discharge into the channel defined by

$$q_i'' = \frac{q_i}{(KL/\rho c_p)} = \frac{L_e}{L} q_i', \tag{18}$$

where q_i is the discharge per unit width in the inflow current at $x = 0$, and q_i' is defined by (13). In figure 3 the closed-form solution for θ_0 is compared with the author's data

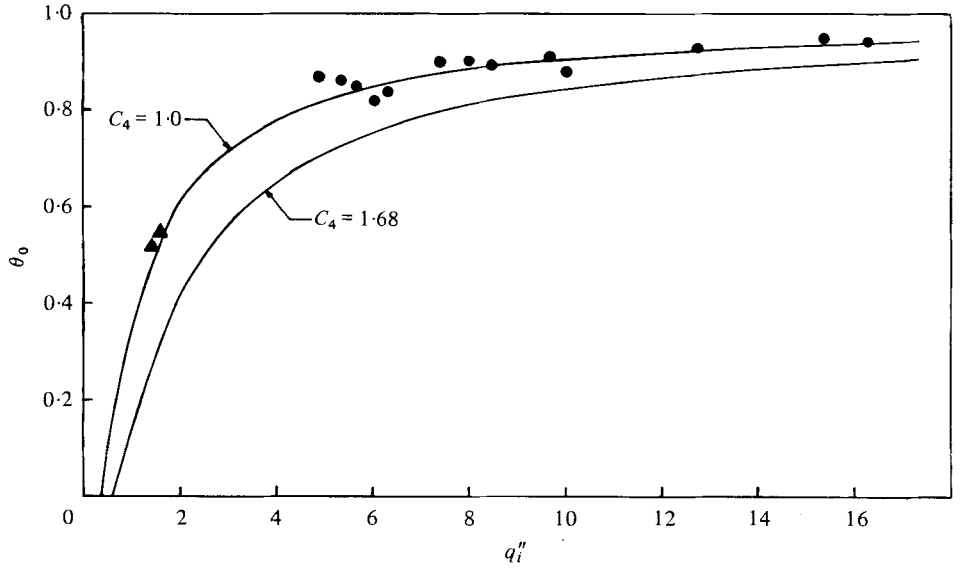

FIGURE 10. Comparison of closed-form solution for boundary values θ_0 and q_i'' [$= q_i/(KL/\rho c_p)$] with experimental values. ●, Brocard *et al.* (1977) [$f_T(\eta) = \eta^4$]; ▲, author's results [$f_T(\eta) = \eta^5$].

and selected data of Brocard *et al.* for which the height of the point of inflection in the temperature profiles measured from the channel bottom varied from 0·55 to 0·65 times the depth. This allowed each data set to be plotted according to a single temperature profile shape, which was chosen to be $f_T(\eta) = \eta^4$ for the selected data of Brocard *et al.* and $f_T(\eta) = \eta^5$ for the author's data. The influence of the chosen temperature profile shape appears in the value of L_e and hence in the plotting position of the experimental data along the horizontal axis in figure 3. The solution curves for θ_0 and H' are unaffected by temperature profile shape.

The experimental values of q_i'' are plotted *vs.* the corresponding experimental values of θ_0 in figure 10. Such a functional relation follows from (18) and the observation that, in figure 3, θ_0 and q_i' are both functions of L/L_e. The values of K in the measured q_i'' are based on empirical relationships for the surface heat loss at the air–water interface and are calculated by $K = -\phi_{ni}/(T_i - T_e)$, where ϕ_{ni} is the rate of heat loss per unit area at $x = 0$. The surface-heat-loss relations used in the reduction of the author's data shown in figure 10 were adjusted from those suggested by Brocard *et al.* for their data such that the heat loss calculated from the measured water temperatures along the entire channel agreed with the measured rate of heat input. If the relations of Brocard *et al.* had been used instead to determine K, the author's data points would be shifted to the right by approximately 30 per cent and slightly downward in figure 10.

The general trend of the solution curves agrees well with the experimental data in figures 3 and 10, but there is scatter about the curve for θ_0, and the dimensionless discharge is consistently overestimated. This latter discrepancy may be due in part to the difficulty and associated error in measuring the discharge q_i, but the influence of the chosen temperature profile shape probably plays a greater role. The measured temperature profiles in figure 6, for example, are considerably 'fuller' than the higher-degree polynomial shapes given by $f_T(\eta)$, which were selected for ease of integration

in obtaining the closed-form solution. The result is that the interfacial friction is probably underestimated by the closed-form solution and agreement with the measured values of θ_0 is obtained by over-compensating with a higher degree temperature polynomial to get a reasonable value of C_1, which appears in (11). An additional solution curve is shown in figure 10 for C_4 arbitrarily chosen to be 1·0 to show the better agreement with the experimental data that can be obtained. Because of the strong dependence of C_4 on the temperature profile shape and the estimate of the order of magnitude of the inertia terms given in § 4, the discrepancy between the closed-form solution and the experimental results is thought to be influenced primarily by the temperature profile shape rather than by neglecting the inertia terms in the momentum equation.

An additional difficulty in expressing the experimental results for q_i' is the problem of experimentally determining the linear coefficient K for an inherently nonlinear relation between the rate of surface heat loss and surface temperature. The combined choice of K and temperature profile shape for the experimental results in figures 3 and 10 seems to have produced values of Ra_m and L/L_e which give reasonable agreement between the measured and calculated θ_0 but the corresponding values of q_i', which also involve K in their definition, are overestimated by the closed-form solution.

7. Summary and conclusions

It has been shown that a closed-form solution of the coupled equations of motion and thermal energy reproduces the essential aspects of laboratory results for thermally induced gravity currents in the laminar regime. The governing dimensionless parameter of the problem is a modified Rayleigh number, which is shown to determine not only the solutions for temperature, velocity, and depth, but also the initially unknown velocity and temperature boundary conditions. The results of the closed-form solution are limited by the assumption of laminar flow and the relatively simple shapes chosen for the temperature profiles, but the solution provides a foundation for the understanding of the mechanics of thermally induced gravity currents under less limited circumstances.

The experimental portion of this investigation was carried out at the Iowa Institute of Hydraulic Research, and the author is indebted to Professor J. F. Kennedy for many useful discussions. The analytical work reported in this paper was completed at the Georgia Institute of Technology with partial support from National Science Foundation Grant ENG 78-21957.

Appendix. Definition of profile constants

$$C_1 = \left(\int_0^1 f_T(\eta) f_u(\eta)\, d\eta \right)^{-1},$$

$$C_2 = 3 \int_0^1 \int_0^\eta [f_1(\eta) - f_1(1)]\, d\eta\, d\eta,$$

$$C_3 = C_1 f_u(1), \quad C_4 = C_1 \int_{h/D}^1 f_u(\eta)\, d\eta,$$

where

$$f_1(\eta) = \int_0^\eta \int_1^\eta f_T(\eta)\, d\eta\, d\eta,$$

$$f_u(\eta) = -\int_0^\eta \int_1^\eta \int_1^\eta f_T(\eta)\, d\eta\, d\eta\, d\eta - \frac{C_2}{2}\eta^2 + C_2\eta.$$

REFERENCES

BENJAMIN, T. B. 1968 Gravity currents and related phenomena. *J. Fluid Mech.* **31**, 209–248.

BROCARD, D. N., JIRKA, G. H. & HARLEMAN, D. R. F. 1975 Buoyancy driven circulations in side-arms of cooling lakes. *Proc. A.S.C.E. National Convention, Denver, Colorado.*

BROCARD, D. N., JIRKA, G. H. & HARLEMAN, D. R. F. 1977 A model for the convective circulation in side-arms of cooling lakes. *Ralph M. Parsons Lab. for Water Resources and Hydrodynamics Rep.* no. 223. Massachusetts Institute of Technology.

CORMACK, D. E., LEAL, L. G. & IMBERGER, J. 1974 Natural convection in a shallow cavity with differentially heated end walls. Part 1. Asymptotic theory. *J. Fluid Mech.* **65**, 209–229.

IMBERGER, J. 1974 Natural convection in shallow cavity with differentially heated end walls. Part 3. Experimental results. *J. Fluid Mech.* **65**, 247–260.

KEULEGAN, G. H. 1957 An experimental study of the motion of saline water from locks into fresh water channels. *Nat. Bur. Stand. Rep.* 5168.

KOH, R. C. Y. 1966 Viscous stratified flow towards a sink. *J. Fluid Mech.* **24**, 555–575.

KREITH, F. 1973 *Principles of Heat Transfer*, p. 392. Intext Press.

PHILLIPS, O. M. 1966 On turbulent convection currents and the circulation of the Red Sea. *Deep Sea Res.* **13**, 1149–1160.

RYAN, P. J., HARLEMAN, D. R. F. & STOLZENBACH, K. D. 1974 Surface heat loss from cooling ponds. *Water Resources Res.* **10**, 930–938.

STURM, T. W. 1976 An analytical and experimental investigation of density currents in side-arms of cooling ponds. Ph.D. thesis, University of Iowa.

TURNER, J. S. 1973 *Buoyancy Effects in Fluids*, p. 87. Cambridge University Press.